Journal of Molecular Structure 1161 (2018) 89–99

Contents lists available at ScienceDirect

Journal of Molecular Structure

journal homepage: http://www.elsevier.com/locate/molstruc

Synthesis, characterization, experimental and theoretical structure of novel Dichloro(bis{2-[1-(4-methoxyphenyl)-1H-1,2,3-triazol-4-yl-κN^3]pyridine-κN})metal(II) compounds, metal = Mn, Co and Ni

J. Conradie [a, *], M.M. Conradie [a], K.M. Tawfiq [b, c], M.J. Al-Jeboori [c], S.J. Coles [d], C. Wilson [e], J.H. Potgieter [b, f, **]

[a] Department of Chemistry, University of the Free State, P.O. Box 339, Bloemfontein, 9300, South Africa
[b] Division of Chemistry and Environmental Science, Manchester Metropolitan University, Manchester, M1 5GD, UK
[c] Department of Chemistry, College of Education for Pure Science (Ibn Al-Haitham), University of Baghdad, Baghdad, Iraq
[d] EPSRC National Crystallography Service, Chemistry, University of Southampton, Southampton, SO17 1BJ, England, UK
[e] School of Chemistry, University of Glasgow, Joseph Black Building. University Avenue, Glasgow, G12 8QQ, Scotland, UK
[f] School of Chemical and Metallurgical Engineering, University of the Witwatersrand, Private Bag X3, Wits, 2050, South Africa

ARTICLE INFO

Article history:
Received 20 December 2017
Received in revised form
4 February 2018
Accepted 8 February 2018
Available online 9 February 2018

Keywords:
(1,2,3-Triazol-4-yl)pyridine
Manganese
Cobalt
Nickel
DFT

ABSTRACT

The syntheses, characterizations and structures of three novel dichloro(bis{2-[1-(4-methoxyphenyl)-1H-1,2,3-triazol-4-yl-κN^3]pyridine-κN})metal(II), [M(L)$_2$Cl$_2$], complexes (metal = Mn, Co and Ni) are presented. In the solid state the molecules are arranged in infinite hydrogen-bonded 3D supramolecular structures, further stabilized by weak intermolecular π…π interactions. The DFT results for all the different spin states and isomers of dichloro(bis{2-[1-phenyl-1H-1,2,3-triazol-4-yl-κN^3]pyridine-κN}) metal(II) complexes, [M(L^1)$_2$Cl$_2$], support experimental measurements, namely that (i) d^5 [Mn(L^1)$_2$Cl$_2$] is high spin with S = 5/2; (ii) d^7 [Co(L^1)$_2$Cl$_2$] has a spin state of S = 3/2, (iii) d^8 [Ni(L^1)$_2$Cl$_2$] has a spin state of S = 1; and (iv) for all [M(L^1)$_2$Cl$_2$] and [M(L)$_2$Cl$_2$] complexes, with M = Mn, Co and Ni, the *cis-cis-trans* and the *trans-trans-trans* isomers, with the pyridyl groups *trans* to each other, have the lowest energy.

1. Introduction

There are many sources of energy alternative to conventional fossil fuels. One of these is the photovoltaic cell. Current commercial photovoltaic devices are most commonly silicon based solid state cells. The main aim in the development of photovoltaic cells is to achieve the highest possible efficiency, converting as much sunlight as possible to electrical energy, whilst also keeping the cost to a minimum to ensure affordability for commercial use. One such development in this area is the Dye-sensitized solar cell (DSSC). DSSCs are the most efficient 3rd generation photovoltaic devices and were first proposed by Michael Grätzel in 1991 [1]. The DSSC has 5 main components, a semiconductor, transparent conducting layer, sensitized dye, electrolyte and a counter electrode. The process of energy conversion is triggered when the dye is exposed to sunlight. Being photosensitive, the dye molecule enters an excited state, promoting an electron from the HOMO to the LUMO. This results in the injection of the electron into the conduction band of the semiconductor and this oxidises the dye. The sensitized dye is then reduced and immediately regenerated when it accepts an electron from the redox couple in the electrolyte. The electrolyte is subsequently reduced by the counter electrode or cathode. This regeneration process allows the sustained conversion of light energy [2]. There are a number of criteria which the sensitized dye must fulfil in order to be deemed suitable for use in a DSSC. Firstly, it should be able to absorb all wavelengths of light below 920 nm. Secondly, there needs to be a good anchoring group present, allowing it to bind firmly and irreversibly, through the process of chemisorption, to the semiconductor. Also, if the electron density is centred on the anchoring group, there will be a more efficient electron injection to the semiconductor. With regards to energy levels, the LUMO of the dye should be above the conduction

* Corresponding author. Department of Chemistry, University of the Free State, P.O. Box 339, Bloemfontein, 9300, South Africa.
** Corresponding author. Division of Chemistry and Environmental Science, Manchester Metropolitan University, Manchester, M1 5GD, UK.
E-mail address: conradj@ufs.ac.za (J. Conradie).

https://doi.org/10.1016/j.molstruc.2018.02.036
0022-2860/

band edge of the semiconductor whilst the HOMO energy level should be below that of the redox electrode [3]. Ruthenium is the most commonly utilised metal in sensitized dyes [4,5]. DSSCs utilise extrinsic semiconductors which can be found as two types. Firstly there is an n-type semiconductor, the most popular choice which utilises wide band-gap metal oxides such as TiO_2 and ZnO_2. The second type, the p-type, makes use of metal oxides such as NiO. N-type semiconductors have a large electron concentration compared to p-type semiconductors. The most popular semiconductor used in DSSCs is TiO_2, because it provides the highest efficiencies [6]. There are a couple of key requirements which an electrolyte must fulfil to increase the efficiency in a DSSC. Firstly, fast dye regeneration and secondly, slow electron recapture are essential. The most commonly used electrolyte is tri-iodide (I^{3-})/iodide (I^-) due to it fulfilling the necessary criteria. However, there are a few disadvantages to using iodine based electrolytes, including the inability to absorb light of wavelengths other than blue. This causes a decrease in the short circuit photocurrent and thus reduces the power conversion efficiency of the cell [7].

Cobalt complexes have been shown to be quite suitable when used as a DSSC electrolyte. Yella et al. [8] used a Co(II/III) tris(bipyridyl)–based electrolyte coupled with a zinc-porphyrin sensitized dye and managed to achieve a power conversion efficiency of 12.3%. Similarly, Yum et al. [9] tested a few different Co(II/III)tris(bipyridyl)–based electrolytes and discovered that they had a very high open circuit voltage, whilst also maintaining a low short circuit current. When used in conjunction with an organic sensitized dye, they produced a power conversion efficiency of greater than 10%. By using a tris(1,2-diaminoethane)cobalt(II)/(III) electrolyte in a p-type cell, Powar et al. [10] managed to obtain power conversion efficiencies of 1.3% and a very high open circuit voltage of 709 mV. Whilst this is relatively high for a p-type cell, about 2.3 times greater than the previous best performing p-type DSSCs, it is still quite low compared to n-type cells. However, whilst not being sufficiently efficient on their own, p-type cells could possibly be used in conjunction with n-type compounds to give better performance.

Triazole-containing dyes showed promising results to be used in DSSC [11]. Triazole-functionalized BODIPY dyes prove to be useful probes for monitoring amyloid conformational transitions in vitro [12]. Ru derivative chromophores may be very promising for the photoinduced nonlinear optics [13]. We recently reported on a series of differently substituted 1,2,3-triazole chromophores [14]. Here we present and compare the structure, chemical and electronic properties of a series of pyridyl-triazole based transition metal complexes, namely d^5 Mn(II), d^7 Co(II) and d^8 Ni(II), for potential use as a sensitized dye in DSSCs. We complexed the 1,2,3-triazole chromophores 2-(1-(4-methoxyphenyl)-1H-1,2,3-triazol-1-yl)pyridine to the first row transition metals Mn, Co and Ni (Fig. 1).

2. Methods and materials

2.1. Synthesis of the 2-(1-(4-methoxyphenyl)-1H-1,2,3-triazol-1-yl) pyridine-metal complexes [ML_2Cl_2]

The ligand, L = 2-(1-(4-methoxyphenyl)-1H-1,2,3-triazol-1-yl) pyridine, was synthesized and characterized as described previously [14–17]. Standard literature methods were slightly adapted to synthesize the metal-pyridyl-triazole complexes. Generally 1 equivalent of the metal chloride and 2 equivalents of the 2-(1-(4-methoxyphenyl)-1H-1,2,3-triazol-1-yl)pyridine ligand was stirred at room temperature (RT) for 8–10 h in a 1:1 mixture of CH_3OH and DCM as solvent. The solvent was removed under vacuum. The solid mass obtained was then washed with several volumes of cold methanol and diethyl ether [18].

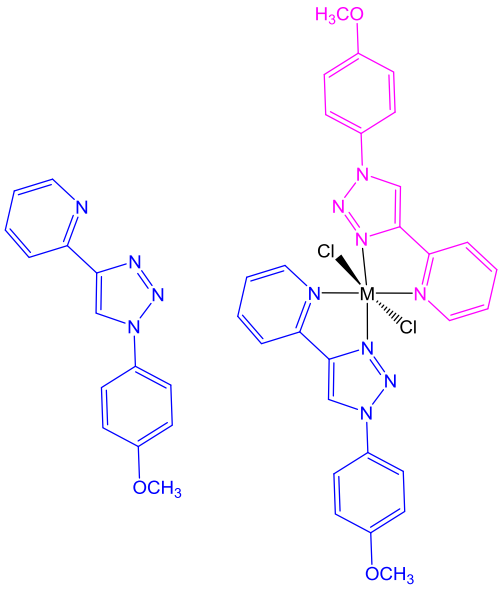

Fig. 1. Structure of 2-(1-(4-methoxyphenyl)-1H-1,2,3-triazol-1-yl)pyridine (L) and its metal(II) complex [ML_2Cl_2]. M = Mn, Co and Ni.

2.1.1. Dichloro(bis{2-[1-(4-methoxyphenyl)-1H-1,2,3-triazol-4-yl-κN^3]pyridine-κN})Manganese(II)

The complex [$Mn(L)_2Cl_2$] was prepared by stirring a solution of anhydrous $MnCl_2$ (0.14 g, 0.11 mmol) in CH_3OH (10 ml). A solution of the ligand L (0.58 g, 0.23 mmol, 2 eq) in CH_2Cl_2 (10 ml), was added dropwise to it. A resulting pale yellow precipitate was obtained after stirring for 8–10 h at RT. The solvent was then reduced in volume by a half under vacuum distillation before it was filtered and washed twice with cold methanol and then diethyl ether. A pale, yellow solid was obtained and isolated to yield a precipitate that give the product (0.14 g, 0.22 mmol, yield 82%), mp. 310–312 °C. IR: $\bar{\upsilon}(cm^{-1})$: 3049, 3025, 2966, 2873, 1604, 1569, 1518, 1471, 1452, 1259, 1203, 1174, 1117, 1066, 1055, 1017, 1001, 980, 864, 827, 786, 751, 718. UV–Vis (DMSO) λ_{max}: The Mn(II) complex showed absorption bands at 258 nm, $\varepsilon_{max} = 6210$ $dm^3mol^{-1}cm^{-1}$, 291 nm, $\varepsilon_{max} = 3059$ $dm^3mol^{-1}cm^{-1}$, 352 nm, $\varepsilon_{max} = 32$ $dm^3mol^{-1}cm^{-1}$, 369 nm, $\varepsilon_{max} = 30$ $dm^3mol^{-1}cm^{-1}$, 390 nm, $\varepsilon_{max} = 21$ $dm^3mol^{-1}cm^{-1}$. $\mu_{eff} = 5.32$ B M. HRMS TOF (ESI+) (water: acetonitrile = 1:3) with the highest molecular weight ion peak matching, was observed at $m/z = 594.1069$ (90%) and is attributed to $[[Mn(L)_2Cl_2] - Cl]^+$. The calculated value for $[(C_{28}H_{24}ClMnN_8O_2)]^+$ is 594.1091. A good single crystal for X-ray structural analysis was obtained by slow evaporation of a hot methanol solution of the complex. Λ_M (DMSO) = 52 $\Omega^{-1}cm^2mol^{-1}$.

2.1.2. Dichloro(bis{2-[1-(4-methoxyphenyl)-1H-1,2,3-triazol-4-yl-κN^3]pyridine-κN})cobalt(II)

For the preparation of [CoL_2Cl_2], the method used was analogous to that for [MnL_2Cl_2]. An amount of $CoCl_2.6H_2O$ of 0.035 g, 0.14 mmol and 0.071 g, 0.32 mmol of L were used, and an identical work-up procedure gave the required compound as a pale pink solid, and the isolated precipitate gave (0.091 g, 0.14 mmol, yield 77%), mp. 340 °C (decomp.). IR: $\bar{\upsilon}(cm^{-1})$: 3068, 3052, 3030, 3014, 2966, 2839, 1609, 1597, 1574, 1518, 1471, 1453, 1320, 1261, 1204, 1175, 1067, 1058, 1019, 1003, 979, 860, 825, 786, 752, 720. UV–Vis (DMSO) λ_{max}: The Co (II) complex showed absorption bands at 257 nm, $\varepsilon_{max} = 26625$ $dm^3mol^{-1}cm^{-1}$, 292 nm, $\varepsilon_{max} = 11000$

$dm^3mol^{-1}cm^{-1}$, 615 nm, $\varepsilon_{max} = 38$ $dm^3mol^{-1}cm^{-1}$, 677 nm, $\varepsilon_{max} = 61$ $dm^3mol^{-1}cm^{-1}$. $\mu_{eff} = 3.97$ B M. HRMS TOF (ESI+) (water: acetonitrile = 1:3) with the highest molecular weight ion peak matching, was observed at $m/z = 598.1048$ (90%) and correspond to $[[CoL_2Cl_2] - Cl]^+$. The calculated value for $[(C_{28}H_{24}ClCoN_8O_2)]^+$ is 598.1043. A good single crystal for X-ray structural analysis was obtained by slow evaporation of a hot DMSO: CH_3CN = 1:9 solution of the complex. Λ_M (DMSO) = 42 $\Omega^{-1}cm^2mol^{-1}$.

2.1.3. Dichloro(bis{2-[1-(4-methoxyphenyl)-1H-1,2,3-triazol-4-yl-κN^3]pyridine-κN})nickel(II)

For the preparation of $[NiL_2Cl_2]$, the method used was similar to that for $[MnL_2Cl_2]$. An amount of $NiCl_2.6H_2O$ of 0.037 g, 0.15 mmol and 0.08 g, 0.31 mmol of L were used, and an identical work-up procedure gave the required compound as a pale blue solid. The isolated precipitate gave (0.073 g, 0.11 mmol, yield 74%), mp. 345 °C (decomp.). IR: ῡ(cm^{-1}); 3073, 3052, 3030, 2985, 2839, 1612, 1597, 1575, 1519, 1473, 1455, 1322, 1263, 1176, 1070, 1060, 1020, 1005, 980, 862, 825, 787, 754, 721. UV–Vis (DMSO) λ_{max}: The Ni (II) complex showed absorption bands at 257 nm, ε_{max}=30000 $dm^3mol^{-1}cm^{-1}$, 291 nm, ε_{max}=18167 $dm^3mol^{-1}cm^{-1}$, 407 nm, ε_{max}=61 $dm^3mol^{-1}cm^{-1}$, 660 nm, ε_{max}=43 $dm^3mol^{-1}cm^{-1}$. μ_{eff} = 2.73 B M. HRMS TOF (ESI+) (water: acetonitrile = 1:3) with the highest molecular weight ion peak matching, was observed at $m/z = 597.1086$ (80%) and is related to $[[NiL_2Cl_2] - Cl]^+$. The calculated value for $[(C_{28}H_{24}ClNiN_8O_2)]^+$ is 597.1064. A good single crystal for X-ray structural analysis was obtained by slow evaporation of a hot DMSO: Acetonitrile = 1:9 solution of the complex. Λ_M (DMSO) = 54 Ω^{-1} cm^2 mol^{-1}.

2.2. Instrumental conditions

Infrared (ATR-FTIR IR) spectra were recorded using a smart diamond ATR attachment on a Thermo -Nicolet FT-IR Spectrometer (AVATAR 320) over the range 4000 to 400 cm^{-1}. Mass spectra were performed at EPSRC Mass Spectrometry Service Centre, University of Wales, Swansea and University of Sheffield. The instrument used was the 'WATERS LCT premier', the ionization was electrospray (ESI+), the solvent was water/acetonitrile (1:3), while the ionization was electrospray (TOF MS ES+). Thermofisher LTQ Orbitrap XL used to analyse volatile molecules in the mass range m/z 50–2000 or m/z 200–4000 Da.

2.3. Magnetic susceptibility

Magnetic susceptibility is measured with a Gouy magnetic susceptibility balance. The gram magnetic susceptibility for a substance is calculated from:

$$\chi_g = (C_{bal})(I)(R\text{-}R_0) \Big/ \left(10^9\right)(m)$$

where l = height of sample in the tube in units of centimeters, m = mass of the sample in units of grams, R = reading for tube plus sample, R_o = reading for the empty tube and C_{bal} = balance calibration constant = 1.0. The molar magnetic susceptibility is then calculated from the gram magnetic susceptibility using the following equation.

$$\chi_m = \left(\chi_g\right)(\text{molar mass})$$

The effective magnetic moment for a particular substance is calculated from the molar magnetic susceptibility [19] using the following equation (T represents the Kelvin temperature (294 K)):

$$\mu_{eff} = 2.83[(\chi_m)(T)]^{1/2}$$

The calculated μ_{eff} values for the $[ML_2Cl_2]$ complexes are given in the experimental characterization data and discussed in section 3.2.

2.4. X-ray diffraction

Single crystal X-ray diffraction measurements for $[MnL_2Cl_2]$, $[CoL_2Cl_2]$ and $[NiL_2Cl_2]$ were performed using a Rigaku Saturn 724 + area detector mounted at the window of an FR-E+ rotating anode generator with Mo Kα, λ = 0.71075 Å. The crystals were mounted on mitegen loops and the data were collected at 100 K under nitrogen flow from an Oxford Cryosystems Cobra device. Data were processed and empirical absorption corrections were also carried out using Crystal Clear SM-Expert [20]. The structures were solved by direct methods using SHELXS (Sheldrick, 2008) [21] within the OLEX2 [22] software. All refinements on F_o^2 by full-matrix least squares refinement were performed using the SHELXL program package (Sheldrick, 2015) [23].

All non-hydrogen atoms were refined with anisotropic displacement parameters and hydrogen atoms were added at calculated positions and included as part of a riding model with C–H (aromatic) 0.95 Å $U_{ISO} = 1.2U_{eq}$ (C); C–H (methyl) 0.98 Å $U_{ISO} = 1.5U_{eq}$ (C) [24]. Perspective drawings of the molecular structures of $[MnL_2Cl_2]$, $[CoL_2Cl_2]$ and $[NiL_2Cl_2]$, also showing the atom numbering scheme used, are shown in Fig. 3, Fig. 4 and Fig. 5. Crystallographic data are presented in Table 3 with selected bond lengths, bond angles and torsion angles in Table 4. Crystallographic data has been deposited at the Cambridge Crystallographic Data Centre with numbers 1818511–1818513. Additional crystallographic data is provided in the Electronic Supplementary Information.

2.5. Theoretical approach

Density functional theory (DFT) calculations were performed unrestricted, in the gas phase, with the B3LYP [25,26] functional as implemented in the Gaussian 09 package [27] using the triple-ζ basis set 6-311G(d,p). Since the complexes of this study are paramagnetic, all the different spin states were considered when performing the DFT calculations. All structures were confirmed as true minimum structures by a frequency analysis, i.e. no imaginary frequencies. The input coordinates for the complexes were constructed using Chemcraft [28].

3. Results and discussion

The 2-(1-(4-methoxyphenyl)-1H-1,2,3-triazol-1-yl)pyridine-metal complexes of this study were synthesized from a 2:1 mol ratio of the 2-(1-(4-methoxyphenyl)-1H-1,2,3-triazol-1-yl)pyridine and the metal chloride. Characterization of the product includes FT-IR, MS, UV–Vis, melting points, magnetic moments, solid state X-ray crystal structures and computational chemistry calculations.

3.1. IR spectral data

The IR spectra of the metal complexes exhibited bands with appropriate shifts due to complex formation (see Table 1 and Supplementary Information Figures S1 – S4). The $\nu(C{=}N)_{py}$ stretching band of the pyridine moiety which is observed at the value around 1604 cm^{-1} in the free ligand, is shifted to higher wavenumbers, around 1612–1607 cm^{-1} for the various complexes. This indicates coordination of the nitrogen of the C=N pyridine

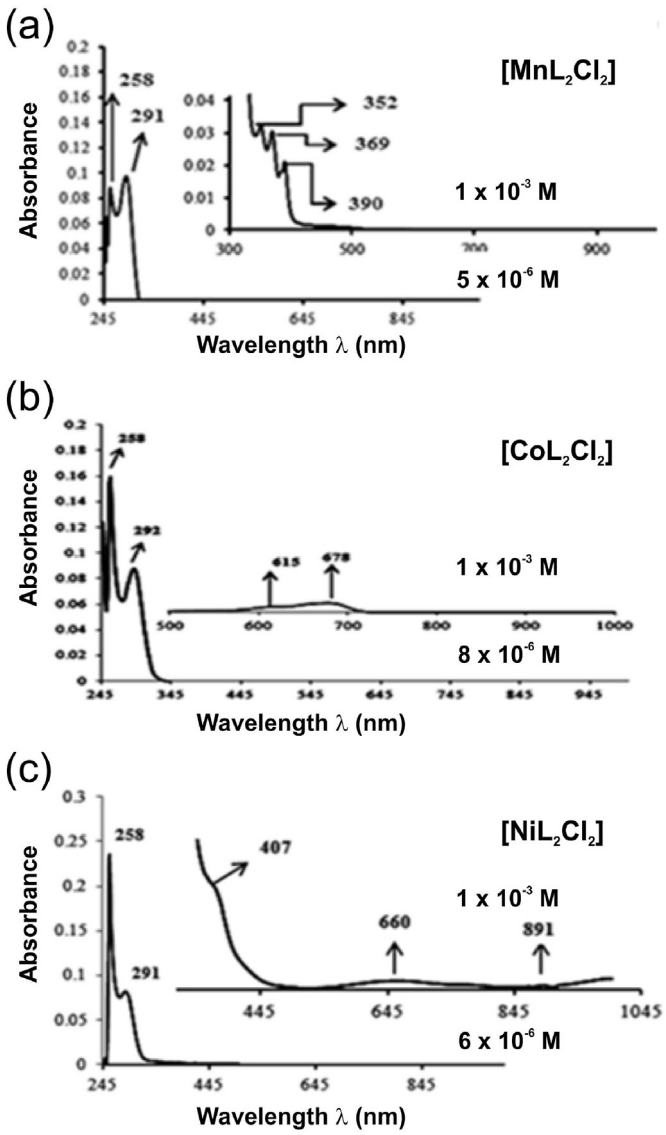

Fig. 2. UV–Vis spectra of the $[ML_2Cl_2]$ complex in DMSO solutions.

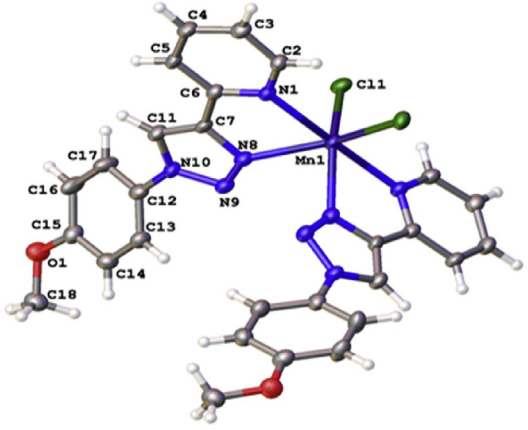

Fig. 3. A labelled molecular structure diagram of $[MnL_2Cl_2]$ with displacement thermal ellipsoids drawn at 50% probability.

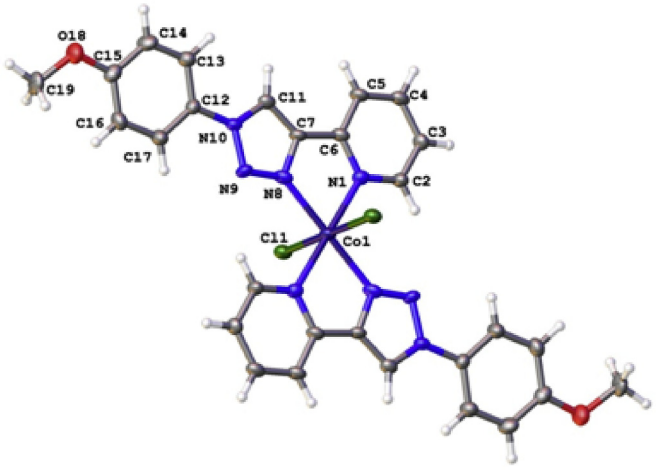

Fig. 4. A labelled molecular structure diagram of $[CoL_2Cl_2]$ with displacement thermal ellipsoids drawn at 50% probability. The asymmetric unit consists of one half of the complex with the other half generated by symmetry and the Co atom lying on an inversion centre.

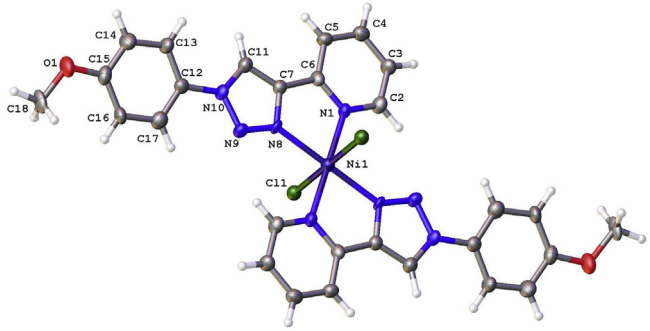

Fig. 5. The molecular structure of $[NiL_2Cl_2]$. The thermal ellipsoids are drawn at a 50% probability. The asymmetric unit consists of one half of the complex with the other half generated by symmetry and the Ni atom lying on an inversion centre.

moiety to the different metal atoms. The $\nu(C{=}C)_{Ar}$ bands of the phenyl ring for the complexes, which usually appear as two absorptions are around 1598-1580 cm^{-1} and 1500-1470 cm^{-1}, compared with the peak at 1592 cm^{-1} in the free ligand [29,30]. The $\nu(C{=}N)_{triaz}$ absorption band of the triazole moiety around 1574 cm^{-1} in the free ligand is detected around 1569–1575 cm^{-1} in the metal complexes, while the $\nu(C{=}C)_{triaz}$ absorption band of the triazole moieties which appear at 1549 cm^{-1} in the free ligand, is detected around 1551–1557 cm^{-1} in the metal complexes, as indicated in Table 1.

3.2. Magnetic moment

The d^5 $[MnL_2Cl_2]$, d^7 $[CoL_2Cl_2]$ and d^8 $[NiL_2Cl_2]$ are paramagnetic and cannot be characterized by NMR. The magnetic moment values obtained for the complexes are given in Table 2. The observed room temperature magnetic moment value of 5.32 B M for d^5 $[MnL_2Cl_2]$ is typical for a high spin configuration of Mn(II)-complexes, and confirm an octahedral geometry about Mn atom [31–33]. The magnetic measurement of the spin (d^7) Co(II) complex, with the value 3.97 B M, corresponds to three unpaired electrons. This value is in agreement with a high spin configuration and supports an octahedral environment around the Co(II) ion [34,35]. The magnetic measurement value 2.73 B M for d^8 $[NiL_2Cl_2]$ corresponds to

Table 1
IR frequencies in wavenumber (cm^{-1}) units of the ligands (L) and the $[ML_2Cl_2]$ complexes.

Compound	ν(C=N)$_{py}$, ν(C=C)$_{Ar,}$ ν(C=N)$_{triaz}$ conj.	ν(C=C)$_{triaz}$	ν(N–N)$_{triaz}$	ν(N=N)$_{triaz}$	ν(C–N)
L	1604, 1592, 1574	1549	1154,1022	1515	1258
$[Mn(L)_2Cl_2]$	1607, –, 1569	1555	1174,1055	1518	1259
$[Co(L)_2Cl_2]$	1609, 1597, 1574	1557	1175,1019	1518	1261
$[Ni(L)_2Cl_2]$	1612, 1597, 1575	1551	1176,1020	1519	1263

two unpaired electrons. This value is in agreement with a high spin configuration and confirmed the octahedral environment around the spin (d^8) Ni(II) atom [36–38].

3.3. UV–vis spectral data

UV–visible spectrometry highlights the differences in the ability of the complexes to absorb light. The UV–Vis Spectrum data of the $[ML_2Cl_2]$ complexes are presented in Table 2 and shown in Fig. 2. The free ligand L, as well as the $[ML_2Cl_2]$ complexes have two intraligand, $\pi \rightarrow \pi^*$, $n \rightarrow \pi^*$ peaks in the 250–300 nm range regardless of the metal centre.

The UV–Vis spectrum of the Mn(II) complex in Fig. 2 (a) exhibits two bands at 258 nm, and 291 nm at concentration of 5×10^{-6} M. These bands are related to the intraligand transitions $\pi \rightarrow \pi^*$ and $n \rightarrow \pi^*$, respectively. High spin Mn(II)-complexes are very weakly coloured compounds due to spin forbidden d-d transitions. Therefore, it is difficult to identify the d-d bands of the Mn(II) complex. At higher concentrations of the Mn(II)-complex, e.g. at a concentration of 1×10^{-3} M, the complex displays several bands. The first band at 352 nm = 28409 cm^{-1}; $\varepsilon_{max} = 32\ dm^3\ mol^{-1}cm^{-1}$, is assignable to an $n \rightarrow \pi^*$ transition. The metal-ligand charge transfer transition band is observed at 369 nm = 27100 cm^{-1}; $\varepsilon_{max} = 30\ dm^3\ mol^{-1}\ cm^{-1}$.

The spectra of the Co(II) complex depicted in Fig. 2 (b), show intraligand transitions. The Co-complex displays two additional bands in the visible region at 615 and 678 nm, which are related to $^4T_1g^{(F)} \rightarrow {}^4T_1g^{(P)}$ and $^4T_1g^{(F)} \rightarrow {}^4A_2g^{(F)}$ transitions respectively. This is characteristic for the distorted octahedral geometry around the Co atom.

In addition to the intraligand transitions, the Ni(II) complex, Fig. 2 (c), has a further two absorbance peaks, the first being at 407 nm and the second at 660 nm, attributed to $^3A_2^{(F)} \rightarrow {}^3T_1^{(P)}$ and $^3A_2g^{(F)} \rightarrow {}^3T_1g^{(F)}$ transitions, respectively. This is typical for a distorted octahedral geometry around the Ni atom [39].

3.4. X-ray structures

The molecular structure of the complexes $[MnL_2Cl_2]$, $[CoL_2Cl_2]$ and $[NiL_2Cl_2]$ can be described as distorted octahedral. The structures of $[CoL_2Cl_2]$ and $[NiL_2Cl_2]$ have the two bidentate triazole ligands in the equatorial plane and the two chloro ligands in the axial positions *trans* to each other. However, in $[MnL_2Cl_2]$, the two chloro ligands are adopting the *cis* positions around the Mn centre. Perspective drawings of the molecular structures, also showing the atom numbering scheme, are given in Fig. 3 (*cis* $[MnL_2Cl_2]$), Fig. 4 (*trans* $[CoL_2Cl_2]$) and Fig. 5 (*trans* $[NiL_2Cl_2]$). Crystallographic data are presented in Table 3 with selected bond lengths, bond angles and torsion angles in Table 4. Additional crystallographic data is provided in the Electronic Supplementary Information. The *trans* $[CoL_2Cl_2]$ and *trans* $[NiL_2Cl_2]$ structures are presented here, while it is the first time that a *cis* orientation of the (1,2,3-triazol-4-yl)pyridine ligands and the halogen atoms has been found for an octahedral Mn(II), Co(II) or Ni(II) complex containing two bidentate (1,2,3-triazol-4-yl)pyridine ligands and two halogen atoms. The only other known crystal structure of an octahedral Mn(II), Co(II) or Ni(II) complex containing two bidentate (1,2,3-triazol-4-yl)pyridine ligands and two halogen atoms [40], is a that of a Ni(II) complex, dibromo(bis{2-[1-(4-cyclohexyl)-1H-1,2,3-triazol-4-yl-κN^3]pyridine-κN})nickel(II), that also has a *trans* orientation of the halogen (bromo) atoms with the triazole ligands in the equatorial plane [41].

3.4.1. Cis $[MnL_2Cl_2]$

Cis $[MnL_2Cl_2]$ crystallised in an orthorhombic space group *Pbcn* with four molecules per unit cell. The geometry about the Mn atom is essentially a distorted octahedral coordination arrangement with a twofold symmetry axis, C_2, through Mn. The octahedral basal plane is formed by the two Cl atoms Cl1 and $Cl1^i$, which are arranged in the *cis* position to each other and two nitrogen atoms N8 and $N8^i$. The remaining two vacant sites on the metal centre are occupied by the nitrogen atoms N1 and $N1^i$ of the pyridyl moieties adopting a *trans* position with a 178.89(16)° angle between $N1^{ax}$–Mn1–$N1i^{ax}$. The ligand-metal-ligand angles in *cis* $[MnL_2Cl_2]$ deviate significantly from the ideal value of 90° or 180° (characteristic of a regular octahedron), see Table 4. The 2-(1-(4-methoxyphenyl)-1H-1,2,3-triazol-1-yl)pyridine ligands fold around the metal ion in a *cis* conformation, allowing the N triazoles to from an equatorial plane with the Cl^- anions. Completing the remaining axial sites on the manganese atom are the N atoms of the

Table 2
UV–Vis spectral data of $[ML_2Cl_2]$ complexes and L in DMSO solutions.

Compound	Band Position λ_{max} (nm)	Wave number (cm^{-1})	Extinction coefficient ε_{max} ($dm^3mol^{-1}cm^{-1}$)	Assignment	μ_{eff} B.M	Conductivity Λ_M ($\Omega^{-1}cm^2mol^{-1}$)
L	285	35087	24375, (4×10^{-6} M)	Intraligand, $\pi \rightarrow \pi^*$, $n \rightarrow \pi^*$		
$[MnL_2Cl_2]$	258, 291	38759, 34364	6210,3059, (5×10^{-6} M)	Intraligand, $\pi \rightarrow \pi^*$, $n \rightarrow \pi^*$	5.32	52
	352,	28409,	32, (1×10^{-3} M)	–		
	369	27100	30, (1×10^{-3} M)	CT		
	390	25641	21, (1×10^{-3} M)	$^6A_{1g} \rightarrow {}^4T_{1g}$		
$[CoL_2Cl_2]$	257, 292	38910, 34246	26625, 11000, (8×10^{-6} M)	Intraligand $\pi \rightarrow \pi^*$, $n \rightarrow \pi^*$	3.97	42
	615	16260	38, (1×10^{-3} M)	$^4T_1g^{(F)} \rightarrow {}^4T_1g^{(P)}$		
	677	14771	61, (1×10^{-3} M)	$^4T_1g^{(F)} \rightarrow {}^4A_2g^{(F)}$		
$[NiL_2Cl_2]$	257, 291	39682, 34364	30000, 18167 (6×10^{-6} M)	Intraligand $\pi \rightarrow \pi^*$, $n \rightarrow \pi^*$	2.73	54
	407	24570	61, (1×10^{-3} M)	$^3A_2^{(F)} \rightarrow {}^3T_1^{(P)}$		
	660	15151	43, (1×10^{-3} M)	$^3A_2g^{(F)} \rightarrow {}^3T_1g^{(F)}$		

Table 3
Crystallographic data for the complexes.

Compound	$[MnL_2Cl_2]$	$[CoL_2Cl_2]$	$[NiL_2Cl_2]$
Empirical formula	$C_{28}H_{24}Cl_2MnN_8O_2$	$C_{28}H_{24}Cl_2CoN_8O_2$	$C_{28}H_{24}Cl_2NiN_8O_2$
M_r	630.39	634.39	634.16
Temp/K	100 K	100(2) K	100(2) K
Cryst. syst.	Orthorhombic	Monoclinic	Monoclinic
Space group	*Pbcn*	$P2_1/c$	$P2_1/c$
a/Å	13.4618(9)	10.3480(10)	10.459(15)
b/Å	9.2130(6)	12.9032(12)	12.968(17)
c/Å	22.9298(16)	10.1969(9)	10.350(15)
α/°	90.00	90.00	90.00
β/°	90.00	95.772(7)°	95.61(3)
γ/°	90.00	90.00	90.00
V/Å^3	2843.8(3)	1354.6(2)	1397(3)
Z	4	2	2
R_{int}	0.1012	0.2085	0.1445
D_{calcd}/g cm^{-3}	1.472	1.555	1.508
Refln (all/ind/obsd)	12965/ 3242	15422/ 3098/1250	7036/ 3134
μ/mm^{-1}	1.000–0.092	0.875	0.928
*R*1 (obsd data: $F^2 > 2\sigma(F^2)$)[a]	0.0597/ 0.1345	0.047	0.0928/ 0.1629
w*R*2 (all data)[a]	0.1127/ 0.1624	0.089	0.1772/ 0.2084

Table 4
Selected experimental bond lengths (Å), bond and torsion angles (°) for the $[ML_2Cl_2]$ complexes and the L ligand.

	L	$[MnL_2Cl_2]$	$[CoL_2Cl_2]$	$[NiL_2Cl_2]$
Bond distance (Å)				
C7–C11	1.362(6)	1.371(5)	1.360(4)	1.361(9)
N8–N9	1.302(4)	1.305(4)	1.308(4)	1.331(7)
N9–N10	1.355(4)	1.358(4)	1.362(3)	1.369(7)
N8–C7	1.365(5)	1.365(4)	1.360(3)	1.369(8)
M–$N_{(PY)}$1		2.330(3)	2.127(2)	2.109(6)
M–$N_{(triazole)}$8		2.324(3)	2.105(3)	2.091(5)
M–Cl1		2.4544(11)	2.4398(10)	2.454(3)
Bond angle (°)				
$N_{(PY)}$1–M–$N_{(PY)}1^i$		178.89(16)	180.0	180.0
$N_{(triazole)}8^i$–M–$N_{(triazole)}$8		87.13(15)	180.	180.0
$N_{(PY)}$1–M–$N_{(triazole)}8^i$		108.95(11)	102.92(10)	101.3(2)
$N_{(PY)}$1–M–$N_{(triazole)}$8		71.90(10)	77.08(10)	78.7(2)
$N_{(PY)}$1–M–Cl1		91.05(8)	90.31(8)	90.29(15)
$N_{(PY)}1^i$ –M–Cl1		88.30(8)	89.69(8)	89.71(15)
$N_{(triazole)}8^i$ –M–Cl1		155.71(8)	90.26(9)	89.33(18)
$N_{(triazole)}$8–M–Cl1		86.19(8)	89.74(9)	90.67(18)
$Cl1^i$–M–Cl1		108.66(6)	180.0	180.0
Torsion angle (°)				
$N_{(triazole)}8^i$–M–$N_{(PY)}$1–C2		96.3(3)	0.6 (3)	1.8(6)
$N_{(triazole)}$8–M–$N_{(PY)}$1–C2		176.6(3)	−179.4(3)	−178.2(6)
$Cl1^i$–M–$N_{(PY)}$1–C2		10.9(3)	90.9(3)	92.4(5)
Cl1–M–$N_{(PY)}$1–C2		−97.8(3)	−89.91(3)	−87.6(5)
$N_{(triazole)}8^i$–M–$N_{(triazole)}$8–N9		−75.5(3)	–	–
$N_{(PY)}$1–M–$N_{(triazole)}$8–N9		173.5(4)	179.6(4)	179.7(6)
$N_{(PY)}$1i–M–$N_{(triazole)}$8–N9		−5.8(4)	0.4(4)	−0.3(6)
$Cl1^i$–M–$N_{(triazole)}$8–N9		−149.7(3)	−89.2(4)	−90.5(6)
Cl1–M–$N_{(triazole)}$8–N9		81.1(3)	90.8(4)	89.5(6)
M–$N_{(triazole)}$8–N9–N10		−160.6(3)	177.0(3)	176.8(4)
N8–N9–N10–C11		−0.4(4)	−0.3(4)	0.4(7)
N8–N9–N10–C12		−179.8(3)	179.2(3)	−179.7(5)

pyridyl moieties.

The bite angle N8–Mn–N1 within the coordinated 2-(1-(4-methoxyphenyl)-1H-1,2,3-triazol-1-yl)pyridine ligands is 71.90(10)°. Consequently the Cl1–Mn1–Cl1 angle of 108.66(6)° is slightly higher than the angles found for octahedral Mn(II) complex having *cis* chloride atoms (for example CSD reference codes CIQWUW, MAMNCH, PYMNCH10, QUMNCL, TMAMNC, YAJTUA with angles between 89 and 96° [40,42]). The bond length of the terminal chloro groups, Mn–Cl1 and Mn–$Cl1^i$, is 2.4544(11) Å. The bond lengths of N8–N9, N9–N10 and N8–C7 of the 1,2,3-triazole segment are 1.305(4) Å, 1.358 (4) and 1.365(5) Å, respectively. These distance values are similar to the distances for the free ligand, namely 1.302(4) Å, 1.355(4) Å and 1.365(5) Å respectively. The Mn–N_{PY} and Mn–$N_{triazole}$ bond lengths of 2.330(3) Å and 2.324(3) Å are within normal values [43–45].

The angles between the pyridine plane and the triazole ring and between the triazole plane and the substituted phenyl ring are 115.4(3)° and 120.5(3)°, respectively. The dihedral angle between the plane of the pyridyl moiety and the mean plane of the triazole ring is 5.4(5)°. Furthermore, the dihedral angle between the plane of methoxy phenyl group and the plane of the triazole moiety is tilted by 38.6(5)°.

In the crystal a range of interactions lead to the 3D supramolecular structure; CH···O, CH···N and CH···Cl as well as π…π interactions are all present. The chelated (triazole) segment is involved in a (C–H …N) interaction which forms sheets in the *ab* plane perpendicular to the c-axis while CH···O(methoxy) interactions form sheets in the ac plane perpendicular to the b-axis and link the CH···N sheets to give a 3D structure. There are three CH···Cl contacts, similar to those in the Ni and Co structures (see next section), which form a 3D network with angles at the Cl atom ranging from 90° to 130° [46,47]. There is an offset-slipped parallel alignment of the phenyl rings, stabilized by phenyl-phenyl π…π interactions between the ($C_{12}C_{13}C_{14}C_{15}C_{16}C_{17}$) and the ($C_{12}C_{13}C_{14}C_{15}C_{16}C_{17}$) phenyl rings with a centroid – centroid distance of 3.985 Å and a plane to centroid distance of 3.68 Å. Details are given in Table 5 and Fig. 6.

3.4.2. *Trans* $[CoL_2Cl_2]$ and *trans* $[NiL_2Cl_2]$

The X-ray molecular structure of *trans* $[CoL_2Cl_2]$ (Fig. 4) and

Table 5
Intermolecular interaction parameters; D = donor and A = acceptor (Å, °) in the complex $[MnL_2Cl_2]$.

D–H … A	D–H	H–A	D–A	Angle
C3–H3···O1	0.950(4)	2.510(3)	3.540 (8)	159.0(2)
C18–H18A … Cl1	0.981(4)	2.882(9)	3.700(4)	141.4(2)
C5–H5···Cl1	0.950(3)	2.685(1)	3.620 (4)	168.3(2)
C11–H11··· Cl1	0.950(4)	2.599(8)	3.490(1)	156.2(4)
Mn–Cl···H5				96.75(4)
Mn–Cl···H11				115.89(4)
Mn–Cl···H18A				91.59(3)

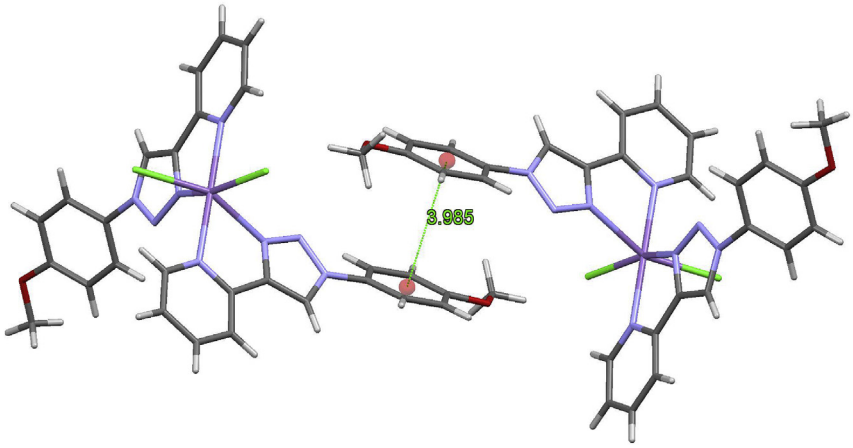

Fig. 6. Partial packing in $[MnL_2Cl_2]$ showing ($\pi \ldots \pi$) stacking interactions. Color code: ($C_{12}C_{13}C_{14}C_{15}C_{16}C_{17}$) centroids (red dots), Cl (green balls), C (grey), N (blue), O (red) and H (white). (For interpretation of the references to colour in this figure legend, the reader is referred to the Web version of this article.)

trans $[NiL_2Cl_2]$ (Fig. 5) are identical as can be seen from molecular structure overlay of the two molecules in Fig. 7 (top). Both compounds crystallise in the monoclinic $P2_1/c$ space group with a distorted octahedral coordination arrangement round the metal, and two molecules per unit cell. Due to inversion symmetry through the metal centre, the asymmetric unit consists of one half of the complex with the other half generated by inversion symmetry. The six atoms coordinated to the metal centre are Cl1 and $Cl1^{i}$, $N8_{triazole}$ and $N8^{i}_{triazole}$, $N1_{PY}$ and $N1^{i}_{PY}$. Nitrogens $N8_{triazole}$ and $N1_{PY}$ belong to the triazole and pyridyl groups of the bidentate 2-(1-(4-methoxyphenyl)-*1H*-1,2,3-triazol-4-yl) pyridine ligand L. In the equatorial plane, the pyridine $N1_{PY}$ and $N8_{triazole}$ donors from the two ligands are mutually *trans* to each other. The angles between the different nitrogens in the equatorial plane, namely $N8^{eq}_{triazole}$ $-M-N1^{e}_{PY}{}^{q}$ and $N8^{i,eq}_{triazole}$ $-M-N1^{eq}_{PY}$ are 77.08(10)° and 102.92(10)° for Co and 78.7(2)° and 101.3(2)° for Ni respectively. These angles between the different nitrogens in the equatorial plane, deviate from the 90° angle for an ideal octahedron, because of the chelating nature of the two L ligands. The axial positions are occupied by two chloride ions Cl1–Ni–$Cl1^{i}$, and due to inversion symmetry, the angle is 180.0° for both structures. The X-ray molecular structure of *trans* $[CoL_2Cl_2]$ and *trans* $[NiL_2Cl_2]$ are very similar (compare the data in Table 4). The dihedral angle between the mean plane of the pyridyl moiety and the mean plane of the triazole ring in the coordinated 2-(1-(4-methoxyphenyl)-1H-1,2,3-triazol-1-yl)pyridine ligand is 0.38° for $[CoL_2Cl_2]$ and 1.68° for $[NiL_2Cl_2]$, allowing conjugation throughout the triazole–pyridyl backbone. The angle between the near planar pyridine-triazole plane and the 4-methoxyphenyl ring is 13.15° for $[CoL_2Cl_2]$ and 15.62° for $[NiL_2Cl_2]$. The X-ray molecular structure of *trans* $[CoL_2Cl_2]$ and *trans* $[NiL_2Cl_2]$ are very similar to that of the related *trans* dibromo(bis{2-[1-(4-cyclohexyl)-1H-1,2,3-triazol-4-yl-κN^3]pyridine-κN})nickel(II) structure [41], containing cyclohexyl instead of the *para*-ethoxyphenyl group-attached at the N10 nitrogen of the triazole group, see Fig. 7 (bottom).

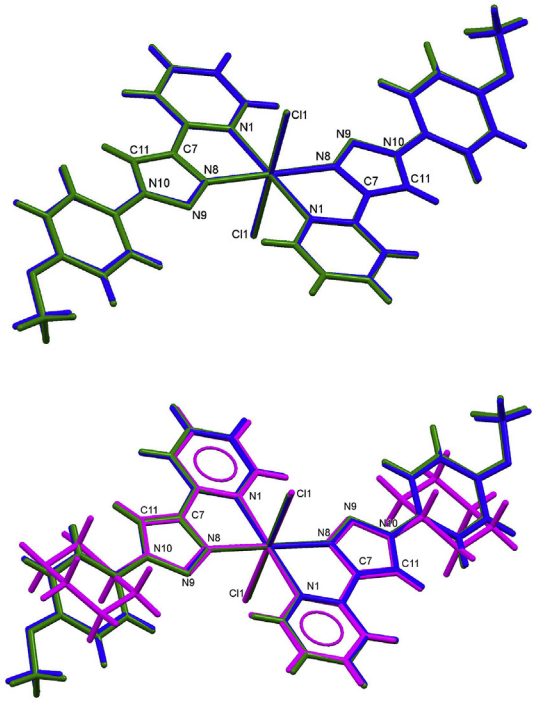

Fig. 7. Top. Overlay of the structures of *trans* $[CoL_2Cl_2]$ (blue) and *trans* $[NiL_2Cl_2]$ (green). The root means square (RMS) overlay values, when using the six atoms of the octahedral coordination polyhedron, is 0.038. Bottom. Overlay *trans* $[CoL_2Cl_2]$ (blue), *trans* $[NiL_2Cl_2]$ (green), and *trans* dibromo(bis{2-[1-(4-cyclohexyl)-1H-1,2,3-triazol-4-yl-κN^3]pyridine-κN})nickel(II) (magenta) [41]. (For interpretation of the references to colour in this figure legend, the reader is referred to the Web version of this article.)

The bond lengths of N8–N9, N9–N10 and N8–C7 of the 1,2,3-triazole ring in the free ligand are very similar to the related bonds in the $[ML_2Cl_2]$ complexes, only in $[NiL_2Cl_2]$ these values are slightly higher (by approximately 0.02 Å), see values in Table 4. In the *trans* $[ML_2Cl_2]$ complexes (M = Co or Ni), the Ni–Cl bond lengths varies from 2.44 to 2.45 Å, the Ni–N_{PY} bond lengths from 2.11 to 2.13 Å, while the Ni–$N_{triazole}$ bond lengths are between 2.09 and 2.11 Å. In a specific complex the metal-triazole bond length is slightly shorter than the metal-pyridine bond length (by approximately 0.02 Å).

An extensive network of weak intermolecular interactions [48] [49], generates a 3D supramolecular structure in the solid state for both $[CoL_2Cl_2]$ and $[NiL_2Cl_2]$. The intermolecular bonding can be described as follows for $[CoL_2Cl_2]$ (similar for $[NiL_2Cl_2]$):

(a) Each chloride atom of one molecule is weakly hydrogen–bonded to two molecules in the next layer, namely (i) C19–H19 of the methoxy group (2.916 Å) of one molecule and (ii) to the C11–H11 on a triazole ring (2.549 Å) and (iii) C13–H13 of the phenyl ring (2.852 Å) of a second

molecule, see Fig. 8. All these are below the sum of the Van der Walls radii of H and Cl of 3 Å [50].

(b) Further weak hydrogen bonds link the C18–H18 of the methoxy group and N9 of the a triazole ring (2.589 Å) of an adjacent molecule, see Fig. 8. The latter N–H interaction is also below sum of the Van der Walls radii of H and N of 2.75 Å.

The overlap between the triazole $N_8N_9N_{10}C_7C_{11}$ and pyridine $N_1C_2C_3C_4C_5C_6$ rings of the neighbouring molecules resulted in face–to–face and slipped-type parallel alignment. The interaction between the molecules are further strengthened by triazole – pyridine and triazole – phenyl π…π stacking of 3.545 Å and 4.149 Å respectively for $[CoL_2Cl_2]$ (Fig. 9) and 3.589 Å and 4.258 Å respectively for $[NiL_2Cl_2]$. This distance is comparable to the previously reported bond separations of a typical π…π stacking [51–54].

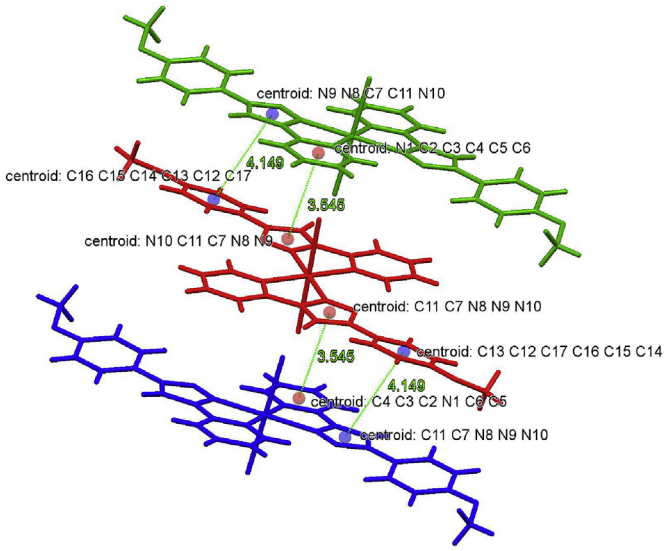

Fig. 9. Partial packing diagram of $[CoL_2Cl_2]$ showing π…π stacking (distance in Å) involving the triazole - pyridyl and phenyl - triazole rings.

3.5. DFT study

Five geometrical isomers, three *cis* and two *trans*, are possible for the metal complexes of this study, containing two bidentate (1,2,3-triazol-4-yl)pyridine ligands and two chloride atoms. The isomers are defined by the relative positions of (i) the chloro atoms, (ii) the pyridyl nitrogen and (iii) the triazole nitrogen around the metal, see Fig. 10. Experimental magnetic moment measurements showed that the three $[ML_2Cl_2]$ complexes of this study are all paramagnetic. To support the experimental assignment of the spin state of the complexes, computational chemistry calculations using density functional theory (DFT) calculations have been done for all the possible spin states of each isomer of the dichloro{bis[2-(1-phenyl-1H-1,2,3-triazol-4-yl-κN^3)pyridine-κN]}metal(II), $[M(L^1)_2Cl_2]$, without a methoxy substituent on the phenyl ring (L^1 = 2-(1-phenyl-1H-[1,2,3-triazol]-4-yl)pyridine). The DFT results, summarized in Table 6, support experimental measurements, showing that:

(i) d^5 $[Mn(L^1)_2Cl_2]$ is high spin with S = 5/2, i.e. five unpaired electrons,

(ii) d^7 $[Co(L^1)_2Cl_2]$ has a spin state of S = 3/2, i.e. three unpaired electrons,

(iii) d^8 $[Ni(L^1)_2Cl_2]$ has a spin state of S = 1, i.e. two unpaired electrons and

(iv) for all $[M(L^1)_2Cl_2]$ complexes, the either *cis-cis-trans* or the *trans-trans-trans* isomers have the lowest energy. In both these isomers the pyridyl groups are *trans* to each other.

For $[Mn(L^1)_2Cl_2]$, the *cis-cis-trans* isomer is preferred by about 0.15 eV, in agreement with the *cis* $[MnL_2Cl_2]$ structure obtained in this study. The *trans-trans-trans* isomer is preferred by a very small

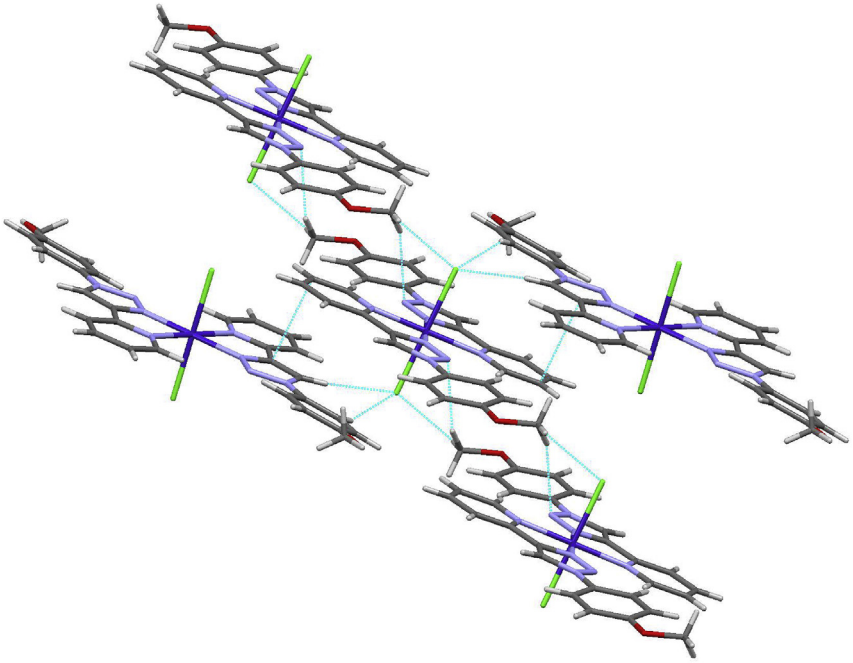

Fig. 8. Partial packing diagram of $[CoL_2Cl_2]$ showing selected intermolecular hydrogen bonding interactions to chloride and CH_3···N interactions.

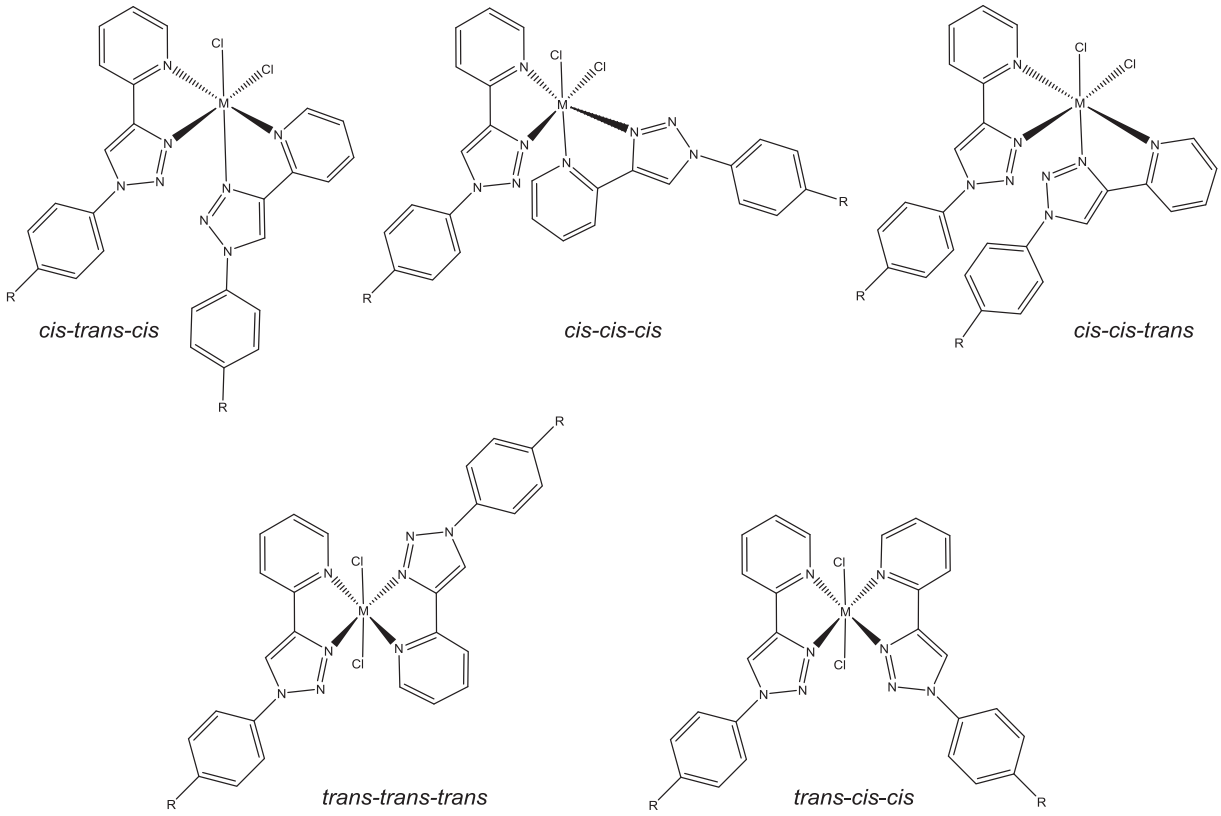

Fig. 10. The five geometrical isomers possible for $[ML_2Cl_2]$ complexes. R = H for L^1 = 2-(1-phenyl-1H-[1,2,3-triazol]-4-yl)pyridine) and R = OCH_3 for L = 2-(1-(4-methoxyphenyl)-1H-1,2,3-triazol-1-yl)pyridine.

Table 6
Relative Electronic energy ΔE and Gibbs energy ΔG for the indicated spin states and geometrical isomers of $[M(L^1)_2Cl_2]$. L^1 = 2-(1-phenyl-1H-[1,2,3-triazol]-4-yl)pyridine. The energy of the lowest energy isomer is indicated in bold font.

Isomer[a]	S	ΔE (eV)	ΔG (eV)	ΔE (eV)	ΔG (eV)	S	ΔE (eV)	ΔG (eV)
		Mn		Co			Ni	
ctc	1/2	1.90	2.11	1.07	1.12	0	1.20	1.20
ccc		1.69	1.92	0.80	0.88		1.21	1.25
cct		1.49	1.72	0.71	0.79		0.97	1.03
ttt		1.35	1.57	0.56	0.64		0.93	0.95
tcc		1.64	1.87	0.74	0.79		1.11	1.09
ctc	3/2	1.78	1.80	0.45	0.43	1	0.50	0.50
ccc		c	c	0.24	0.24		0.29	0.29
cct		c	c	0.04	0.05		0.06	0.07
ttt		2.19	2.34	**0.00**	**0.00**		**0.00**	**0.00**
tcc		1.64	1.74	0.22	0.20		0.25	0.25
ctc	5/2	0.33	0.31					
ccc		0.17	0.15					
cct		**0.00**	**0.00**					
ttt		0.14	0.07					
tcc		b	b					

[a] See Fig. 10 for the geometry of the different isomers, R = H.
[b] Optimized to the *cct* isomer.
[c] Geometry did not converge.

amount of energy (less than 0.07 eV) for $[Co(L^1)_2Cl_2]$ and $[Ni(L^1)_2Cl_2]$.

Additional DFT calculations for the lowest energy spin state of each isomer of the dichloro{bis[2-(1-(4-methoxyphenyl)-1H-1,2,3-triazol-4-yl-κN^3)pyridine-κN]}metal(II), $[M(L)_2Cl_2]$, with a methoxy substituent on the phenyl ring (L = 2-(1-(4-methoxyphenyl)-1H-[1,2,3-triazol]-4-yl)pyridine), Table 7, are in agreement with the conclusions above. The lowest energy isomer for $[Mn(L)_2Cl_2]$,

Table 7
Relative Electronic energy ΔE and Gibbs energy ΔG for the indicated spin states and geometrical isomers of $[M(L)_2Cl_2]$. L = 2-(1-(4-methoxyphenyl)-1H-1,2,3-triazol-1-yl)pyridine. The energy of the lowest energy isomer is indicated in bold font.

Isomer[a]	ΔE (eV)	ΔG (eV)	ΔE (eV)	ΔG (eV)	ΔE (eV)	ΔG (eV)
	Mn S = 5/2		Co S = 3/2		Ni S = 1	
ctc	0.33	0.30	0.43	0.40	0.49	0.46
ccc	0.16	0.15	0.24	0.22	0.29	0.28
cct	**0.00**	**0.00**	0.04	0.02	0.06	0.05
ttt	0.14	0.10	**0.00**	**0.00**	**0.00**	**0.00**
tcc	b	b	0.24	0.21	0.27	0.25

[a] See Fig. 10 for the geometry of the different isomers, R = CH_3.
[b] optimized to the lowest energy *cct* isomer.

$[Co(L^1)_2Cl_2]$ and $[Ni(L^1)_2Cl_2]$ is the *cis-cis-trans*, *trans-trans-trans* and *trans-trans-trans* isomer respectively, in agreement with the experimental structures presented in this study.

It must be noted, however, that the DFT calculated energy differences between the *cis-cis-trans* and *trans-trans-trans* isomers is small. For example, an energy difference of 0.05 eV or 0.10 eV give a population of 12.5% and 2% respectively according to the Boltzmann equation, implying that both isomers should experimentally be possible.

4. Conclusions

Three new first row high spin, octahedral metal(II) complexes containing the 2-(1-(4-methoxyphenyl)-1H-1,2,3-triazol-1-yl)pyridine chromophore as bidentate ligand (L), have been synthesized and fully characterized. DFT results support experimental measurements, that the metal(II) complexes are high spin. DFT

calculations further showed that the *cis-cis-trans* and the *trans-trans-trans* isomers, with the pyridyl groups *trans* to each other, are the lowest in energy, and that both isomers should experimentally be possible. The experimental molecular structures of $[CoL_2Cl_2]$ and $[NiL_2Cl_2]$ have the two bidentate triazole ligands in the equatorial plane and the two chloro ligands in the axial positions *trans* to each other (*trans-trans-trans* isomers), while in $[MnL_2Cl_2]$, the two chloro ligands are adopting the *cis* positions around the Mn centre (*cis-cis-trans* isomer).

Acknowledgements

The National Mass Spectroscopy Centre at the University of Wales, Swansea is thanked for supplying the mass spectrometry data. KT expresses his gratitude to the Iraqi Government for financial support to conduct the research reported in the UK. This work has received support from the South African National Research Foundation and the Central Research Fund of the University of the Free State, Bloemfontein, South Africa. The High Performance Computing facility of the University of the Free State and the Centre for High Performance Computing CHPC of South Africa are gratefully acknowledged for computer time. We thank the EPSRC for funding the UK National Crystallography Service.

Appendix A. Supplementary data

Supplementary data related to this article can be found at https://doi.org/10.1016/j.molstruc.2018.02.036.

References

[1] B. O'Regan, M. Grätzel, A. Low-Cost, High-efficiency solar cell based on dye-sensitized colloidal TiO_2 films, Nature 353 (1991) 737–740, https://doi.org/10.1038/353737a0.
[2] K. Hara, S. Mori, Dye-sensitized solar cells, in: A. Luque, S. Hegedus (Eds.), Handbook of Photovoltaic Science and Engineering, second ed., John Wiley & Sons, West Sussex, UK, 2011, pp. 642–674.
[3] M. Grätzel, Dye-sensitized solar cells, J. Photochem. Photobiol. C Photochem. Rev. 4 (2003) 145–153, https://doi.org/10.1016/S1389-5567(03)00026-1.
[4] G.C. Vougioukalakis, A.I. Philippopoulos, T. Stergiopoulos, P. Falaras, Contributions to the development of ruthenium-based sensitizers for dye-sensitized solar cells, Coord. Chem. Rev. 255 (2011) 2602–2621, https://doi.org/10.1016/j.ccr.2010.11.006.
[5] C.Y. Chen, M.K. Wang, J.Y. Li, N. Pootrakulchote, L. Alibabaei, C.H. Ngoc-le, J.D. Decoppet, J.H. Tsai, C. Grätzel, C.G. Wu, S.M. Zakeeruddin, M. Grätzel, Highly efficient light-harvesting ruthenium sensitizer for thin-film dye-sensitized solar cells, ACS Nano 3 (2009) 3103–3109, https://doi.org/10.1021/nn900756s.
[6] A. Hagfeldt, G. Boschloo, L. Sun, L. Kloo, H. Pettersson, Dye-sensitized solar cells, Chem. Rev. 110 (2010) 6595–6663, https://doi.org/10.1021/cr900356p.
[7] M. Wang, C. Grätzel, S.M. Zakeeruddin, M. Grätzel, Recent developments in redox electrolytes for dye-sensitized solar cells, Energy Environ. Sci. 5 (2012) 9394–9405, https://doi.org/10.1039/C2EE23081J.
[8] A. Yella, H.-W. Lee, H.N. Tsao, C. Yi, A.K. Chandiran, M.K. Nazeeruddin, E.W.-G. Diau, C.-Y. Yeh, S.M. Zakeeruddin, M. Grätzel, Porphyrin-sensitized solar cells with cobalt (II/III)-based redox electrolyte exceed 12 percent efficiency, Science 334 (2011) 629–634, https://doi.org/10.1126/science.1209688.
[9] J.-H. Yum, E. Baranoff, F. Kessler, T. Moehl, S. Ahmad, T. Bessho, A. Marchioro, E. Ghadiri, J.-E. Moser, C. Yi, MdK. Nazeeruddin, M. Grätzel, A cobalt complex redox shuttle for dye-sensitized solar cells with high open-circuit potentials, Nat. Commun. 3 (2012) 631, https://doi.org/10.1038/ncomms1655.
[10] S. Powar, T. Daeneke, M.T. Ma, D. Fu, N.W. Duffy, G. Götz, M. Weidelener, A. Mishra, P. Bäuerle, L. Spiccia, U. Bach, Highly efficient *p*-type dye-sensitized solar cells based on tris(1,2-diaminoethane)cobalt(II)/(III) electrolytes, Angew. Chem. Int. Ed. 52 (2012) 602–605, https://doi.org/10.1002/anie.201206219.
[11] T. Duan, K. Fan, Y. Fu, C. Zhong, X. Chen, T. Peng, J. Qin, Triphenylamine-based organic dyes containing a 1,2,3-triazole bridge for dye-sensitized solar cells via a 'Click' reaction, Dyes Pigments 94 (2012) 28–33, https://doi.org/10.1016/j.dyepig.2011.11.008.
[12] N.W. Smith, A. Alonso, C.M. Brown, S.V. Dzyuba, Triazole-containing BODIPY dyes as novel fluorescent probes for soluble oligomers of amyloid Abeta1-42 peptide, Biochem. Biophys. Res. Commun. 391 (2010) 1455–1458, https://doi.org/10.1016/j.bbrc.2009.12.091.
[13] A. Migalska-Zalas, Z. Sofiani, B. Sahraoui, I.V. Kityk, V. Yuvshenko, J.-L. Fillaut, J. Perruchon, T.J.J. Muller, $\chi(2)$ grating in Ru derivative chromophores incorporated within the PMMA polymer matrices, J. Phys. Chem. B 108 (2004) 14942–14947, https://doi.org/10.1021/jp048794h.
[14] K.M. Tawfiq, G.J. Miller, M.J. Al-Jeboori, P.S. Fennell, S.J. Coles, G.J. Tizzard, C. Wilson, J.H. Potgieter, Comparison of the structural motifs and packing arrangements of six novel derivatives and one polymorph of 2-(1-phenyl-1*H*-1,2,3-triazol-4-yl)pyridine, Acta Cryst. B 70 (2014) 379–389, https://doi.org/10.1107/S2052520614001152.
[15] F. Alonso, Y. Moglie, G. Radivoy, M. Yus, Click chemistry from organic halides, diazonium salts and anilines in water catalysed by copper nanoparticles on activated carbon, Org. Biomol. Chem. 9 (2011) 6385–6395, https://doi.org/10.1039/C1OB05735A.
[16] I.S. Park, M.S. Kwon, Y. Kim, J.S. Lee, J. Park, Heterogeneous copper catalyst for the cycloaddition of azides and alkynes without additives under ambient conditions, Org. Lett. 10 (2008) 497–500, https://doi.org/10.1021/ol702790w.
[17] H. Park, The extraterritoriality of US patents on the pharmaceutical industry, Pharm. Patent. Anal. 3 (2014) 491–498, https://doi.org/10.4155/ppa.14.33.
[18] J.D. Crowley, P.H. Bandeen, L.R. Hanton, A one pot multi-component CuAAC "click" approach to bidentate and tridentate pyridyl-1,2,3-triazole ligands: synthesis, X-ray structures and copper(II) and silver(I) complexes, Polyhedron 29 (2010) 70–83, https://doi.org/10.1016/j.poly.2009.06.010.
[19] G.A. Bain, J.F. Berry, Diamagnetic corrections and Pascal's constants, J. Chem. Educ. 85 (2008) 532–536, https://doi.org/10.1021/ed085p532.
[20] Rigaku Corporation, CrystalClear-SM Expert 2.0 R13 Software for Diffractometer, 2011.
[21] G.M. Sheldrick, A short history of SHELX, Acta Cryst. Sect. A 64 (2008) 112–122, https://doi.org/10.1107/S0108767307043930.
[22] O.V. Dolomanov, L.J. Bourhis, R.J. Gildea, J.A.K. Howard, H. Puschmann, OLEX2: a complete structure solution, refinement and analysis program, J. Appl. Cryst. 42 (2009) 339–341, https://doi.org/10.1107/S0021889808042726.
[23] G.M. Sheldrick, Crystal structure refinement with SHELXL, Acta Cryst. Sect. C 71 (2015) 3–8, https://doi.org/10.1107/S2053229614024218.
[24] C.F. Macrae, I.J. Bruno, J.A. Chisholm, P.R. Edgington, P. McCabe, E. Pidcock, L. Rodriguez-Monge, R. Taylor, J. van de Streek, P.A. Wood, Mercury CSD 2.0 – new features for the visualization and investigation of crystal structures, J. Appl. Cryst 41 (2008) 466, https://doi.org/10.1107/S0021889807067908.
[25] A.D. Becke, Density-functional thermochemistry. III. The role of exact exchange, J. Chem. Phys. 98 (1993) 5648–5652, https://doi.org/10.1063/1.464913.
[26] C. Lee, W. Yang, R.G. Parr, Development of the Colle-Salvetti correlation-energy formula into a functional of the electron density, Phys. Rev. B 37 (1988) 785–789, https://doi.org/10.1103/PhysRevB.37.785.
[27] M.J. Frisch, G.W. Trucks, H.B. Schlegel, G.E. Scuseria, M.A. Robb, J.R. Cheeseman, G. Scalmani, V. Barone, B. Mennucci, G.A. Petersson, H. Nakatsuji, M. Caricato, X. Li, H.P. Hratchian, A.F. Izmaylov, J. Bloino, G. Zheng, J.L. Sonnenberg, M. Hada, M. Ehara, K. Toyota, R. Fukuda, J. Hasegawa, M. Ishida, T. Nakajima, Y. Honda, O. Kitao, H. Nakai, T. Vreven, J.A. Montgomery Jr., J.E. Peralta, F. Ogliaro, M. Bearpark, J.J. Heyd, E. Brothers, K.N. Kudin, V.N. Staroverov, R. Kobayashi, J. Normand, K. Raghavachari, A. Rendell, J.C. Burant, S.S. Iyengar, J. Tomasi, M. Cossi, N. Rega, J.M. Millam, M. Klene, J.E. Knox, J.B. Cross, V. Bakken, C. Adamo, J. Jaramillo, R. Gomperts, R.E. Stratmann, O. Yazyev, A.J. Austin, R. Cammi, C. Pomelli, J.W. Ochterski, R.L. Martin, K. Morokuma, V.G. Zakrzewski, G.A. Voth, P. Salvador, J.J. Dannenberg, S. Dapprich, A.D. Daniels, Ö. Farkas, J.B. Foresman, J.V. Ortiz, J. Cioslowski, D.J. Fox, Gaussian 09, Revision D.01, Gaussian, Inc., Wallingford, CT, 2009.
[28] http://www.chemcraftprog.com/.
[29] L. Jiang, Z. Wang, S.-Q. Bai, T.S. Andy Hor, "Click-and-click" – hybridised 1,2,3-triazoles supported Cu(I) coordination polymers for azide–alkyne cycloaddition, Dalton Trans. 42 (2013) 9437–9443, https://doi.org/10.1039/C3DT50987G.
[30] S.K. Vellas, J.E.M. Lewis, M. Shankar, A. Sagatova, J.D.A. Tyndall, B.C. Monk, ChM. Fitchett, L.R. Hanton, J.D. Crowley, $[Fe_2L_3]^{4+}$ cylinders derived from bis(bidentate) 2-Pyridyl-1,2,3-triazole "click" ligands: synthesis, structures and exploration of biological activity, Molecules 18 (2013) 6383–6407, https://doi.org/10.3390/molecules18066383.
[31] A.B.P. Lever, Inorganic Electronic Spectroscopy, second ed., Elsevier, New York, 1986, p. 249.
[32] W.H. Mahmoud, G.G. Mohamed, M.M.I. El-Dessouky, Coordination modes of bidentate lornoxicam drug with some transition metal ions. Synthesis, characterization and in vitro antimicrobial and antibreastic cancer activity studies, Spectrochim. Acta Part A 122 (2014) 598–608, https://doi.org/10.1016/j.saa.2013.11.069.
[33] M.S. Refata, N.M. El-Metwaly, Spectral, thermal and biological studies of Mn(II) and Cu(II) complexes with two thiosemicarbazide derivatives, Spectrochim. Acta Part A 92 (2012) 336–346, https://doi.org/10.1016/j.saa.2012.02.041.
[34] N. Raman, S. Sobha, A. Thamaraichelvan, A novel bioactive tyramine derived Schiff base and its transition metal complexes as selective DNA binding agents, Spectrochim. Acta Part A 78 (2011) 888–898, https://doi.org/10.1016/j.saa.2010.12.056.
[35] L.S. Kumar, K.S. Prasad, H.D. Revanasiddappa, B. Vijay, B. Jayalakshmi, Synthesis, characterization and antimicrobial activity of Cu(II), Co(II), Ni(II), Pd(II) and Ru(III) complexes with clomiphene citrate, Chem. Sci. J. CSJ 28 (2011) 1–11. http://astonjournals.com/csj.
[36] E. González, A. Rodrigue-Witchel, C.H. Reber, Absorption spectroscopy of

octahedral nickel(II) complexes: a case study of interactions between multiple electronic excited states, Coord. Chem. Rev. 251 (2007) 351–363, https://doi.org/10.1016/j.ccr.2006.08.011.
[37] S. Chandra, A.K. Sharma, Nickel(II) and copper(II) complexes with Schiff base ligand 2,6-diacetylpyridine bis(carbohydrazone): synthesis and IR, mass, ^{1}H NMR, electronic and EPR spectral studies, Spectrochim. Acta Part A 72 (2009) 851–857, https://doi.org/10.1016/j.saa.2008.12.022.
[38] M.J. Al-Jeboori, A.H. Al-Dujaili, A.E. Al-Janabi, Coordination of carbonyl oxygen in the complexes of polymeric *N*-crotonyl-2-hydroxyphenylazomethine, Transition. Met. Chem. 34 (2009) 109–113, https://doi.org/10.1007/s11243-008-9165-9.
[39] Y.-Z. Tong, Q.-L. Wang, M. Si, J. Qi, S.-P. Yan, G.-M. Yang, P. Cheng, D.-Z. Liao, Crystal structure, spectroscopy and magnetism of trinuclear nickel(II), cobalt(II) complexes and their solid solution, Polyhedron 30 (2011) 3151–3157, https://doi.org/10.1016/j.poly.2011.03.024.
[40] Cambridge Structural Database (CSD), Version 5.38, 2017. May 2017 update, Cambridge, UK.
[41] D. Schweinfurth, C.Y. Su, S.C. Wei, P. Braunsteind, B. Sarkar, Nickel complexes with "click"-derived pyridyl-triazole ligands: weak intermolecular interactions and catalytic ethylene oligomerisation, Dalton Trans. 41 (2012) 12984–12990, https://doi.org/10.1039/C2DT31805A.
[42] R. Dey, D. Ghoshal, Syntheses and characterization of two supramolecular self-assembled Mn(II) compounds using *trans* 4,4′-azobispyridine as a bridging ligand: effect of π–π interactions in the formation of a solid-state structure, Polyhedron 34 (2012) 24–30, https://doi.org/10.1016/j.poly.2011.12.004.
[43] Y. Li, W.-Q. Zou, M.-F. Wu, J.-D. Lin, F.-K. Zheng, Z.-F. Liu, S.-H. Wang, G.-C. Guoa, J.-S. Huang, Hydrothermal syntheses, crystal structures and magnetic properties of four Mn(II) and Co(II) coordination polymers generated from new carboxylate-introduced 1,2,3-triazole ligands, Cryst. Eng. Comm 13 (2011) 3868–3877, https://doi.org/10.1039/C1CE05208J.
[44] E. Hao, Z. Wang, L. Jiao, S. Wang, "Click" tetradentate ligands, Dalton Trans. 39 (2010) 2660–2666, https://doi.org/10.1039/B922043G.
[45] H. Hou, X. Meng, Y. Song, Y. Fan, Y. Zhu, H. Lu, C. Du, W. Shao, Two-Dimensional Rhombohedral Grid Coordination Polymers $[M(bbbt)_2(NCS)_2]_n$ (M = Co, Mn, or Cd; bbbt = 1,1'-(1,4-butanediyl) bis-1*H*-benzotriazole): Synthesis, Crystal Structures, and Third-Order Nonlinear Optical Properties, Inorg. Chem. 41 (2002) 4068–4075, https://doi.org/10.1021/ic0255858.
[46] A. Kovács, Z. Varga, Halogen acceptors in hydrogen bonding, Coord. Chem. Rev. 250 (2006) 710–727, https://doi.org/10.1016/j.ccr.2005.04.031.
[47] L. Brammer, E.A. Bruton, P. Sherwood, Understanding the behavior of halogens as hydrogen bond acceptors, Cryst. Growth Des. 1 (2001) 277–290, https://doi.org/10.1021/cg015522k.
[48] T. Steiner, The hydrogen bond in the solid state, Angew. Chem. Int. Ed. 41 (2002) 48–76, https://doi.org/10.1002/1521-3773(20020104)41:1<48::AID-ANIE48>3.0.CO;2-U.
[49] G.A. Jeffrey, An Introduction to Hydrogen Bonding, Oxford University Press, New York and Oxford, 1997.
[50] C.B. Aakeröy, T.A. Evans, K.R. Seddon, I. Pálinkó, The C–H···Cl hydrogen bond: does it exist, New J. Chem. 23 (1999) 145–152, https://doi.org/10.1039/A809309A.
[51] Y. Yang, P. Du, J. Yang, W.Q. Kan, J.F. Ma, A series of Cu(II) and Cd(II) coordination polymers constructed by 3,5-dinitrosalicylic acid and flexible bis(-triazole) ligands containing different spacers, Cryst. Eng. Commun 15 (2013) 4357–4371, https://doi.org/10.1039/C3CE00034F.
[52] C. Janiak, A critical account on π–π stacking in metal complexes with aromatic nitrogen-containing ligands, J. Chem. Soc., Dalton Trans. (2000) 3885–3896, https://doi.org/10.1039/B003010O.
[53] D. Urankar, A. Pevec, I. Turel, J.G. Košmrlj, Pyridyl conjugated 1,2,3-triazole is a versatile coordination ability ligand enabling supramolecular associations, Cryst. Growth Des. 10 (2010) 4920–4927, https://doi.org/10.1021/cg100993k.
[54] I. Bratsos, D. Urankar, E. Zangrando, P. Genova-Kalou, J. Košmrlj, E. Alessioa, I. Turel, 1-(2-Picolyl)-substituted 1,2,3-triazole as novel chelating ligand for the preparation of ruthenium complexes with potential anticancer activity, Dalton Trans. 40 (2011) 5188–5199, https://doi.org/10.1039/C0DT01807D.